2020 IEEE/RSJ International Conference on Intelligent Robots and Systems (IROS)
October 25-29, 2020, Las Vegas, NV, USA (Virtual)

A Bio–inspired Quadruped Robot Exploiting Flexible Shoulder for Stable and Efficient Walking

Akira Fukuhara[1], Megu Gunji[2], Yoichi Masuda[3], Kenjiro Tadakuma[4], and Akio Ishiguro[1]

***Abstract*— While most modern-day quadruped robots crouch their limbs during the stance phase to stabilize the trunk, mammals exploit the inverted-pendulum motions of their limbs and realize both efficient and stable walking. Although the flexibility of the shoulder region of mammals is expected to contribute to reconciling the discrepancy between the forelimbs and hindlimbs for natural walking, the complex body structure makes it difficult to understand the functionality of animal morphology. In this study, we developed a simple robot model that mimics the flexibility of shoulder region in the sagittal plane, and we conducted a two-dimensional simulation. The results suggest that the flexibility of the shoulder contributes to absorbing the different motions between the forelimbs and hindlimbs.**

I. Introduction

Autonomous quadruped robots have great potential for providing various physical services (e.g., patrolling, delivery, and rescue) and have been developed globally, resulting in the establishment of some commercial robots [1], [2], [3]. As a fundamental locomotor strategy, most modern-day quadruped robots are controlled such that the body trunk is used to maintain their posture and height leveled for stable walking. While maintaining the stability of the trunk unit, each limb should support the body weight when in the crouched posture during the stance period to reduce vertical motion of the shoulder and hip. The stance with a crouched–posture limb requires more energy than that with the elected posture. Therefore, the crouched walking strategy makes energetic issue more serious for the autonomous legged robots to facilitate various services in the real world. Here, the challenge is to simultaneously achieve the efficiency of walking and stability of the trunk.

In contrast to modern–day quadruped robots, animal morphologies are sophisticated, with heterogeneity along the cephalocaudal (head-to-tail) direction, realizing versatile tasks and adaptive locomotion for survive in the world. For example, the head and neck allow animals to recognize as well as approach environment independent of the trunk posture during feeding tasks. Furthermore, Forelimbs and hindlimbs are also specialized [4], [5]: while running and jumping, hindlimbs generate more propulsive force; forelimbs can absorb the impact during landing from elevated places [6], [7], [8], [9]. Our motivation is to understand the functionality of animals' heterogeneous morphology as well as establish a new design principle for agile robots that can perform various tasks in the real worlds.

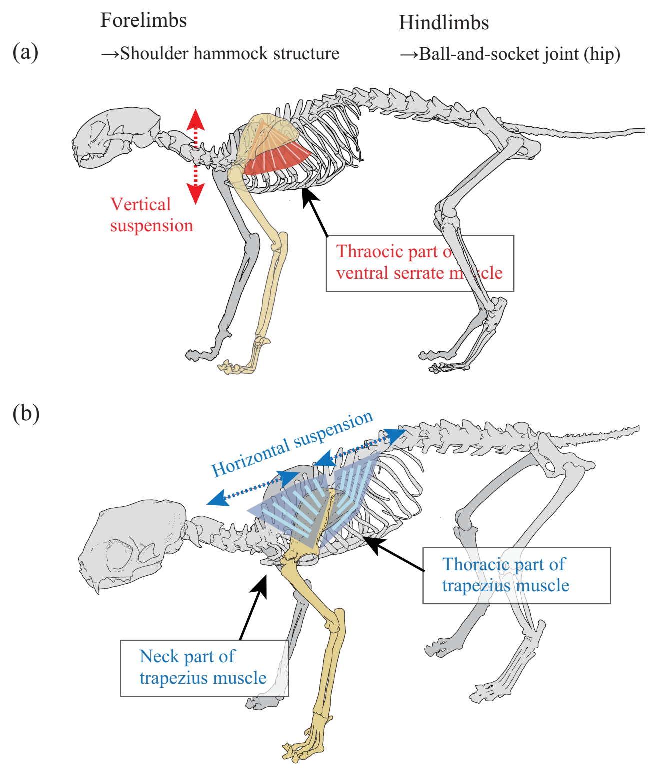

Fig. 1. Anatomical characteristics of quadruped mammals. (a) Thoracic part of ventral serrate muscle. This muscle connects the scapula to the rib cage in the deep layer of the shoulder region, working as vertical suspension of the forelimbs. (b) Trapezius muscle. This muscles connects the scapula to the cervical and thoracic spine, generating horizontal motion of the forelimbs.

The different connectivities to the trunk the forelimbs and hindlimbs is a remarkable heterogeneity in animals' morphology along the cephalocaudal direction. In cursorial mammals, such as cheetahs and horses, there is no skeletal articulation between the forelimbs and the trunk [10]. As shown in Fig. 1 (a), the scapula is connected to the chest through several muscles without skeletal articulations

*This study was supported by the Japan Science and Technology Agency, CREST (JPMJCR14D5) and Tough Cyberphysical AI Research Center, TC-PAI, Tohoku University. This study was also supported by JSPS KAKENHI Grant-in-Aid for Scientific Research on Innovative Areas "Science of Soft Robot" project under Grant Number JP18H05466.

[1]Research Institute of Electrical Communication, Tohoku University, 2-1-1 Katahira, Aoba-ku, Sendai 980-8577, Japan. a.fukuhara@riec.tohoku.ac.jp
[2]National Museum of Nature and Science, Tokyo, 4-1-1 Amakubo, Tsukuba-shi, Ibaraki 305-0005, Japan
[3]Department of Mechanical Engineering, Osaka University, Yamadaoka, Suita, Osaka 565-0871, Japan
[4]Graduate School of Information Sciences Applied Information Sciences, Tohoku University,6-6-01 Aramaki Aza Aoba, Aoba-ku, Sendai-shi, 980-8579, Japan

(i.e., shoulder hammock structure), while the hindlimbs are connected to the pelvis via a deep ball-and-socket joint (i.e., hip joint) [11]. To understand the functionality of the flexible shoulder region, we have developed a quadruped robot mimicking the flexible shoulder and evaluated the functionality under the free-falling task from an elevated place [12]. Although the robot experiments show that flexibility of shoulder allows the robot to redirect the trunk motion from down to up smoothly, the effects of shoulder hammock structure on a walking task are still unclear.

Main contribution of the present study is to investigate effects of flexible shoulder region on stable walking. In walking task, each limb generate inverted–pendulum motions at the shoulder or hip joints. Phase difference between cyclic step motion between limbs will generate discrepancy of vertical motion of the shoulder and hip. We hypothesize that flexibility of the shoulder regions in the sagittal plane can absorbe the the conflict between forelimbs and hindlimbs through the trunk. Thus, we build a simple two-dimensional (2D) simulation, and attempt to establish the relationship between the flexibility of shoulder and locomotor performances. Our results clearly show that the flexible shoulder regions reconcile the inverted–pendulum motions between the forelimbs and hindlimbs, and they suggest the occurrence of stiffness control of the shoulder region depending on the interlimb coordination patterns.

The rest of this paper is organized as follows. Section II explains the anatomical characteristics of quadrupeds and a developed minimal robot model for understanding functionality of shoulder hammock structure in the walking task. Section III shows the results of the simulation experiments. Section IV presents the conclusions and future work.

II. Model

In this section, we consider the minimal element of robot structure to address whether the walking task is moderated by the flexibility in translational motion of the shoulder in the sagittal plane. We first explain the anatomical characteristic of quadrupeds, especially the shoulder region. Then we determine the minimal element for robot design, and develop 2D model for mechanical and control system of the robot.

A. Anatomy of Shoulder Hammock Structure

A significant difference between the forelimbs and hindlimbs is connectivity to the body, as shown in Fig. 1 (a). Hindlimbs are articulated to the pelvis via the deep ball-and-socket (hip) joint, such that the ground reaction force perceived by the hindlimbs would transmit directly to the body, realizing rapid acceleration and large leaping [6], [7], [8]. On the other hand, in the shoulder region of cursorial mammals, the forelimbs connect the chest via some muscles. Such absence of skeletal articulations between the forelimbs and trunk is expected to play different roles from those of the hindlimbs, e.g., shock absorption and maneuverability.

Regarding the details of the pectoral girdle, several muscles connect the forelimbs and chest in different ways [13]. As shown in Fig. 1 (a), thoracic parts of ventral serrate muscles are located in the deep layer, connecting the side of the rib cage and the dorsal region of the medial surface of the scapula. These muscles mainly suspend the chest to support the body weight, i.e., shoulder hammock structure. In contrast, trapezius muscles are located in the superfacial layer, as shown in Fig. 1, and connect the scapula and dorsal region of the trunk along an almost horizontal direction. These superfacial muscles constraint the fore–aft motion of the scapula and actuate to stabilize retracting and protracting motions during the limb stride [14].

Furthermore, there are many other muscles connecting between the forelimb and neck or trunk. For example, the rhomboid muscle, the brachiocephalic muscle, and the omotransverse muscle also connect the forelimb and the neck. Besides, the pectoralis transversus muscle connects the forelimbs and the ventral side of the chest, and generates abduction motion of forelimbs in the transversal plane. Although these muscles support forelimbs, the hardware design may become too complicated to address the flexibility of the shoulder in the sagittal plane. Therefore, we ignore the effect of the neck and the three–dimensional (3D) motion of forelimbs.

From the above, we consider the ventral serrate muscle and trapezius muscle as the minimal anatomical elements to address the flexible translational motion of shoulder in the sagittal plane. For simplicity, we describe the connectivities between forelimbs and chest as two different directions: vertical connection as the ventral serrate muscle and horizontal one as the trapezius muscle.

B. Mechanical System

According to the above simplification, we develop a simple mechanical system of a quadruped robot for 2D simulation as a mass–spring–damper system, as shown in Fig. 2. The robot comprises two forelimbs, two hindlimbs, and a rigid trunk. Each limb has two point masses: m_i^{foot} and m_i^{top}. The parameter i is an index of the limb unit, e.g., for forelimbs, $i = 0,1$, and for hindlimbs, $i = 2,3$. The motion of each limb is generated by two actuators; for example, rotational and prismatic actuators generate the limb stride motion. The body also comprises point masses m_j^{base}, which are connected by rigid prismatic springs and dampers ($K_{\mathrm{pri}}^{\mathrm{fix}}$, $D_{\mathrm{pri}}^{\mathrm{fix}}$), and rigid torsional spring and dampers ($K_{\mathrm{rot}}^{\mathrm{fix}}$ and $D_{\mathrm{rot}}^{\mathrm{fix}}$), respectively. Here, parameter j is an index for body point masses; $j = 0,1,2$ presents the anterior part of the body, while $j = 3,4,5$ represents the posterior part.

Note that each limb is connected to the trunk unit via passive springs, i.e., the hammock structure. A vertical spring and damper correspond to the chest part of the ventral serrate muscle, while the horizontal parts correspond to the trapezius muscle. To address the effects of different connectivities between the fore and hindlimbs, the robot exhibits the hammock structure not only in the shoulder region but also in the hip region. The spring and damper coefficients of the vertical parts of the proximal articulation of the forelimbs (hindlimbs) are described as $K_{\mathrm{v}}^{\mathrm{fore(hind)}}$ and $D_{\mathrm{v}}^{\mathrm{fore(hind)}}$, while

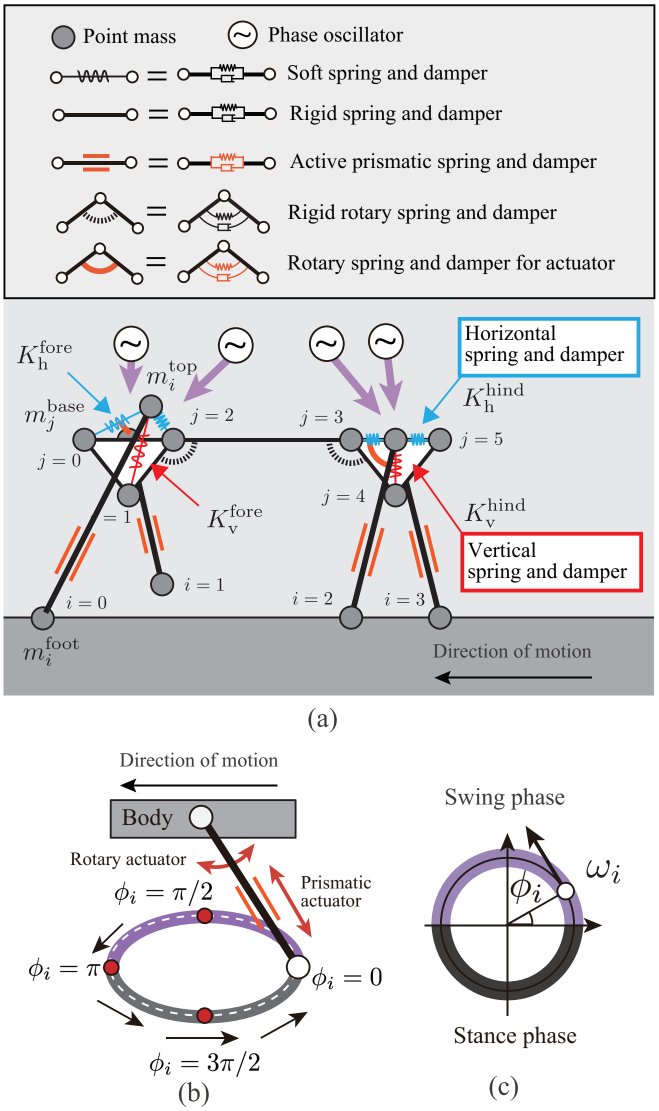

Fig. 2. Mechanical model of a 2D robot. (a) Mass-spring-damper system. Each proximal limb articulation is supported with the vertical and horizontal springs and dampers. (b) Foot trajectory. (c) Phase oscillator for limb control.

the horizontal parts are described as $K_{\mathrm{h}}^{\mathrm{fore(hind)}}$ and $D_{\mathrm{h}}^{\mathrm{fore(hind)}}$, respectively.

The properties of vertical and horizontal parts of the proximal articulation between the limb and trunk detect whether the limb is connected to the trunk via the deep ball-and-socket joint or flexible muscles. For example, high $K_{\mathrm{v}}^{\mathrm{fore(hind)}}$ and $K_{\mathrm{h}}^{\mathrm{fore(hind)}}$ values indicate that the proximal articulation works as the deep ball-and-socket joint, such as a mammal's hip joint. In contrast, the low $K_{\mathrm{v}}^{\mathrm{fore(hind)}}$ and $K_{\mathrm{h}}^{\mathrm{fore(hind)}}$ values indicate that the proximal articulation works as a flexible shoulder region of mammals.

Ground reaction force (GRF) is simplified as follows:

$$N_{\mathrm{v},i} = \begin{cases} -K_{\mathrm{gnd}} y_i - D_{\mathrm{gnd}} \dot{y}_i & (y_i < 0), \\ 0 & (\text{otherwise}), \end{cases} \tag{1}$$

$$N_{\mathrm{h},i} = \mu N_{\mathrm{v},i} (-\tanh \beta \dot{x}_i), \tag{2}$$

where $N_{\mathrm{v},i}$ and $N_{\mathrm{h},i}$ are vertical and horizontal components of GRF applied at the i th limb; K_{gnd} and D_{gnd} are spring and damper coefficients; and y_i and x_i is vertical and horizontal position of foot, respectively. When $D_{\mathrm{gnd}} = 0$, the foot contacts the ground with elastic collision. The horizontal component of the GRF $N_{\mathrm{h},i}$ is modeled as Coulomb friction. A parameter β represents sensitivity of $N_{\mathrm{h},i}$. The parameter μ is a coefficient of friction.

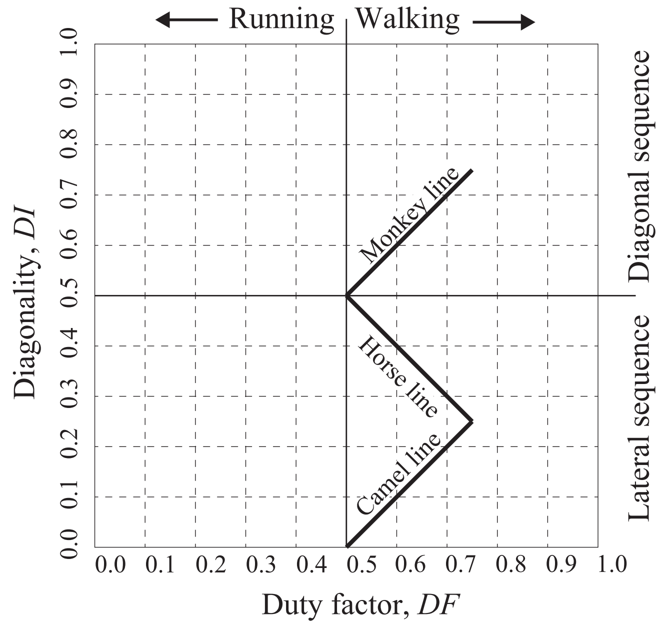

Fig. 3. Hildebrand diagram [15]. Quadruped walking is classified by two fundamental parameters: duty factor (DF) and diagonality (DI). While legged animals exhibit walking gait when $DF < 0.5$, they run as $DF > 0.5$. In terms of diagonality, while almost all mammals exhibit lateral sequence walk ($DI < 0.5$), some primates exhibit diagonal sequence walk ($DI > 0.5$). This figure was drawn in reference to Cartmill et al. [16].

C. Control System

In this study, we evaluate the functionality of the flexible shoulder hammock region during a steady walking task. In the following sections, each stride motion of the limb is explained. Then, interlimb coordination (e.g., gait pattern) is described.

Regarding stride motion of each limb, the foot point–mass m_i^{foot} moves in a specific trajectory, as shown in Fig. 2 (b). The periodic stride motion of the limb is described by a parameter ϕ_i, i.e., the phase of a phase oscillator, as shown in Fig. 2 (c). The phase of oscillator ϕ_i is evaluated as follows:

$$\dot{\phi}_i = \omega_i, \tag{3}$$

where ω_i is the intrinsic angular velocity of the ith limb, which is related to locomotion frequency. When $\phi_i = 0 \sim \pi$, the limb tends to become shorter and move forward, i.e., the swing phase model. In contrast, when $\phi_i = \pi \sim 2\pi$, the limb tends to become longer and move backward, i.e., the stance phase model.

To investigate the functionality of difference in proximal articulation during various walking gait patterns, we describe the interlimb coordination using two fundamental parameters: duty–factor DF and diagonality DI [15], [16]. DF

TABLE I

PARAMETERS IN SIMULATION

body			controller		
parameters	unit	values	parameters	unit	values
m_j^{base}	[kg]	3	ω_{sw}	[rad/s]	7.0
m_i^{foot}	[kg]	0.5	X^{offset}	[m]	0
m_i^{top}	[kg]	0.5	X^{amp}	[m]	0.25
total body mass	[kg]	22.0	Y^{offset}	[m]	0.7
trunk length	[m]	1.3	Y^{amp}	[m]	0.1
leg length	[m]	0.75	Y^{amp}	[m]	0.1
K_{pri}	[N/m]	8.0×10^3	DF		0.7
D_{pri}	[Ns/m]	5.0×10^2	DI		0.3
K_{rot}	[Nm/rad]	3.6×10^3			
D_{rot}	[Nms/rad]	2.3×10^2			
$K_{\mathrm{pri}}^{\mathrm{fix}}$	[N/s]	2.3×10^2			
$D_{\mathrm{pri}}^{\mathrm{fix}}$	[Ns/s]	2.3×10^2			
$K_{\mathrm{rot}}^{\mathrm{fix}}$	[Nm/rad]	2.3×10^2	environment		
$D_{\mathrm{rot}}^{\mathrm{fix}}$	[Nms/rad]	2.3×10^2	parameters	unit	values
$K_{\mathrm{v}}^{\mathrm{fore}}$ (flexible)	[N/m]	5.0×10^3	K_{gnd}	[N/m]	2.0×10^5
$K_{\mathrm{h}}^{\mathrm{fore}}$ (flexible)	[N/m]	2.5×10^3	D_{gnd}	[N/ms]	1.0×10^1
$K_{\mathrm{v}}^{\mathrm{fore}}$ (rigid)	[N/m]	3.0×10^4	μ	[Ns/m]	0.8
$K_{\mathrm{h}}^{\mathrm{fore}}$ (rigid)	[N/m]	1.5×10^4	β	[s/m]	5.0
$K_{\mathrm{v}}^{\mathrm{hind}}$	[N/m]	3.0×10^4			
$K_{\mathrm{v}}^{\mathrm{hind}}$	[N/m]	1.5×10^4			
$D_{\mathrm{v}}^{\mathrm{fore}}$	[Ns/m]	1.5×10^2			
$D_{\mathrm{h}}^{\mathrm{fore}}$	[Ns/m]	1.5×10^2			
$D_{\mathrm{v}}^{\mathrm{hind}}$	[Ns/m]	1.5×10^2			
$D_{\mathrm{h}}^{\mathrm{hind}}$	[Ns/m]	1.5×10^2			

presents the ratio of stance periods during one stride cycle. Here, $DF = T_{st}/(T_{st} + T_{sw})$, where T_{st} is the stance period and T_{sw} is the swing period of one gait cycle. Diagonality presents a stride–lag between a hindlimb and forelimb on the ipsilateral side. If the left and right limbs move in anti-phase, $DI = 0.0$ means pace gait, where the ipsilateral limbs move synchronously. The various walking patterns, e.g., lateral-sequence walk (LS walk) and diagonal–sequence walk (DS walk), are described as $DI = 0.25$ and 0.75, theoretically, as shown Fig. 3. To reflect the fundamental parameters DF and DI into the limb controller, the intrinsic angular velocity ω_i is detected by DF and the initial phase ϕ_i^{init} is detected by DF and DI. The details of parameter detection are explained in Appendix A.

To realize the walking patterns, each limb generates stride motion based on the phase of the oscillator ϕ_i. The limb position is described by ϕ_i, as follows:

$$\bar{x}_i = X^{\mathrm{offset}} + X^{\mathrm{amp}} \cos \phi_i, \tag{4}$$

$$\bar{y}_i = Y^{\mathrm{offset}} + Y^{\mathrm{amp}} \sin \phi_i, \tag{5}$$

where $\bar{x}_i$ and $\bar{y}_i$ are the relative target positions of the feet from the respective shoulder/hip joint, ϕ_i is the phase of the oscillator, X^{offset} and Y^{offset} are constant values representing the center position of the target trajectory, and X^{amp} and Y^{amp} are also constant values denoting the amplitude of the periodic motion of the foot. When $\sin \phi_i > 0$, the limb becomes shorter and tends to lift off the ground (swing phase). When $\sin \phi_i \leq 0$, the limb becomes longer and tends to remain on the ground to support the body (stance phase) (Fig. 2 (b)). According to Equation (4) and (5), the reference angle and length of the prismatic and rotary actuators are calculated as follows:

$$\bar{l}_i = \sqrt{\bar{x}_i^2 + \bar{y}_i^2}, \tag{6}$$

$$\bar{\theta}_i = \sin^{-1}(\bar{y}_i/\bar{l}_i). \tag{7}$$

The torque τ_i and force F_i of the limb are calculated using the following equation:

$$\tau_i = K^{\mathrm{rot}}(\bar{\theta}_i - \theta_i) - D^{\mathrm{rot}}\dot{\theta}_i, \tag{8}$$

$$F_i = K^{\mathrm{pri}}(\bar{l}_i - l_i) - D^{\mathrm{pri}}\dot{l}_i, \tag{9}$$

where K^{rot} and D^{rot} are the spring and damper coefficients of the hip (shoulder) joint of the limb, K^{pri} and D^{pri} are the spring and damper coefficients of the prismatic joint of the limb, θ_i is the actual angle of the hip (shoulder) joint, and l_i is the actual length of the limb.

III. SIMULATION EXPERIMENTS

In this section, we show the 2D simulation conducted to evaluate the effect of the flexible shoulder hammock structure during walking gait. Furthermore, we investigate, by using the developed robot model, why most mammals have flexible proximal articulations in the anterior part of the body (shoulder) and not the posterior part (hip).

A. Reconciliation of Stride Motions between Forelimbs and Hindlimbs by Shoulder Hammock Structure

This simulation experiment aims to understand the effects of the shoulder hammock structure during the walking task. According to our hypothesis, a flexible shoulder can reconcile the different up–down motions between the forelimbs and hindlimbs during walking. As the alternating walk–steps by left and right limbs are described as an inverted pendulum model, a mammals' forelimb unit (i.e., chest) and hindlimbs unit (i.e., hip) also exhibit periodic motion along the vertical direction. Therefore, when the diagonality DI is neither 0.0 nor 0.5, the body should solve discrepancy in vertical motion between the forelimbs and hindlimbs. In such a situation, the flexibility of the shoulder hammock structure would absorb the different motions of limbs, resulting in a smooth walking sequence.

To this end, we set the walking gait as $(DF, DI) = (0.7, 0.3)$, referring the horse line in the Hildebrant diagram as shown in Fig. 3. To address the function of shoulder flexibility, we compare two shoulder properties: for flexible shoulder $(K_{\mathrm{v}}^{\mathrm{fore}}, K_{\mathrm{h}}^{\mathrm{fore}}) = (5.0 \times 10^3, 2.5 \times 10^3)$, whereas for rigid shoulder $(K_{\mathrm{v}}^{\mathrm{fore}}, K_{\mathrm{h}}^{\mathrm{fore}}) = (3.0 \times 10^4, 1.5 \times 10^4)$. Other body and control parameters are set as shown in Table I.

Figure 4 shows the locomotor patterns of the robot with rigid and flexible shoulders. With the rigid shoulder property, proximal articulations at the shoulder and hip regions do not deform, and each limb induces vertical motions of the shoulder and hip, as shown in Fig. 4 (a). Because the anterior and posterior parts of the body move independently, the trunk unit changes its posture largely in the pitch direction after each step. In contrast, the robot with a flexible shoulder exhibits deformation of the shoulder hammock structure in the forelimb step, as shown in Fig. 4 (b), avoiding conflicts between the forelimb and hindlimb motions through the trunk unit. Note that the displacements of the shoulder hammock structure correspond quantitatively to the actual mammals ' behaviors, especially the Felidae family. The locomotion speed of the robot with a flexible shoulder achieved 0.52

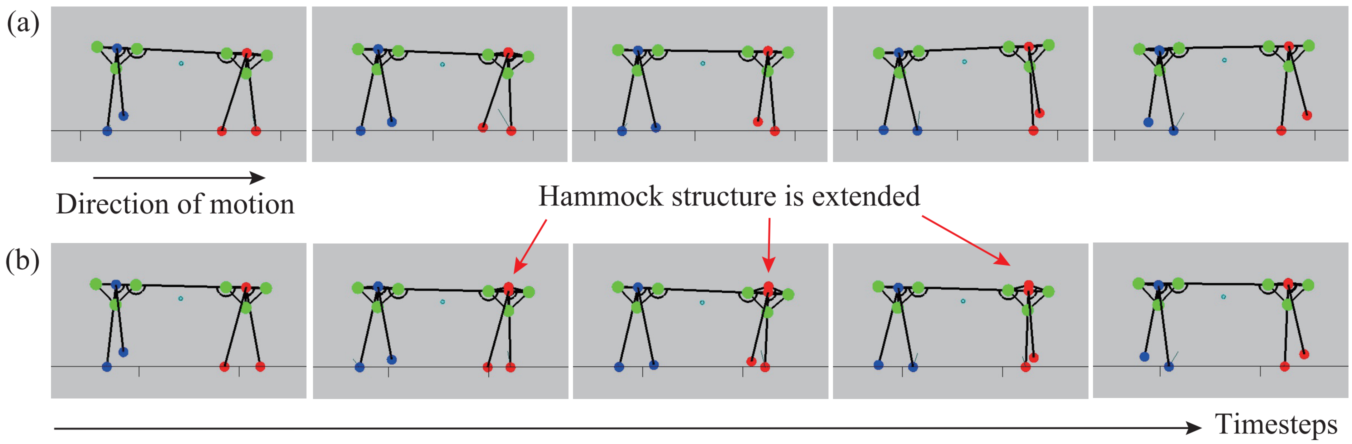

Fig. 4. Snapshots of walking robot (a) with rigid shoulder $(K_v^{\rm fore}, K_h^{\rm fore}) = (3.0\times10^4, 1.5\times10^4)$ and (b) with flexible shoulder hammock structure $(K_v^{\rm fore}, K_h^{\rm fore}) = (5.0\times10^3, 2.5\times10^3)$. The robot with a flexible shoulder structure shows extension of elastic parts during the stance phase of the forelimb. In both simulations, the gait patterns correspond to LS walk, $(DF, DI) = (0.7, 0.3)$, and $\omega_{\rm sw} = 7.0$.

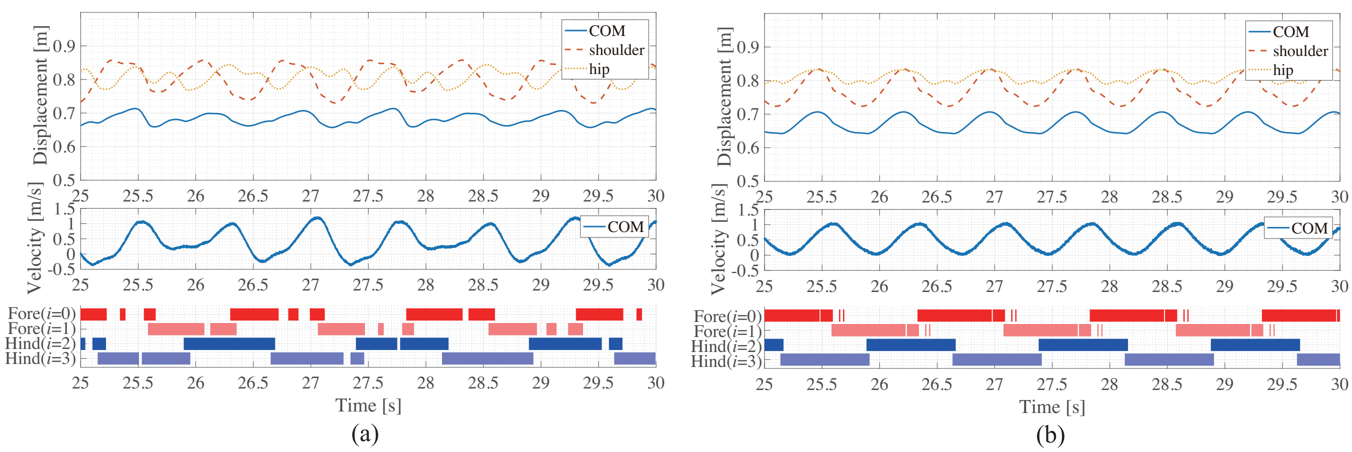

Fig. 5. Changes in height of center of mass (COM) and fore and hindlimbs. (a) Robot with rigid shoulder $(K_v^{\rm fore}, K_h^{\rm fore}) = (3.0\times10^4, 1.5\times10^4)$. (b) Robot with flexible shoulder $(K_v^{\rm fore}, K_h^{\rm fore}) = (5.0\times10^3, 2.5\times10^3)$. The horizontal component of velocity of COM is shown in the middle graph. The colored regions in the gait diagrams indicate that a limb touches the ground.

[m/s], whereas the speed with the rigid one remained at 0.44 [m/s].

Figure 5 shows displacements of the point masses in the trunk unit and gait diagrams during walking with each shoulder property. As shown in Fig. 5, the anterior and posterior parts of the trunk move independently in the vertical direction. Due to the physical conflict between the fore and hind parts, the profile of the COM displacement and gait diagram has small fragments over walking cycles. Regarding the horizontal movements of the robot, the horizontal velocity of COM changes not periodically. In addition, it becomes negative values during the stance of forelimbs. These fact represent the discrepancy in horizontal movements of the robot body. In contrast, the flexible shoulder hammock unit reconciles the inverted–pendulum motions between the forelimbs and hindlimbs, as shown in Fig. 5 (b). The displacement of the anterior trunk engages the posterior part, resulting in smooth motion of the COM and feasible gait diagrams. The horizontal velocity of COM becomes more cyclic than that with the rigid shoulder. Although the velocity still decreases during the middle of the forelimb's stance phase, it keeps positive values.

These results suggest that the flexible shoulder hammock structure contributes to reconciling the inverted–pendulum motions between the forelimbs and hindlimbs during lateral sequence walking.

B. Evaluation of Asymmetry Flexibilities between Shoulder and Hip Regions

The results of the above simulation experiments show the functionality of the shoulder hammock structure during walking. Here, another question arises: why most animals have flexibility in the shoulder region, not the hip region? In this section, we explore the possibility of designing the flexibility of proximal limb joints over various walking patterns. More specifically, we conduct a grid search where the robot walks with various combinations of flexibilities in shoulder and hip regions, and we evaluate it in terms of locomotion speed and

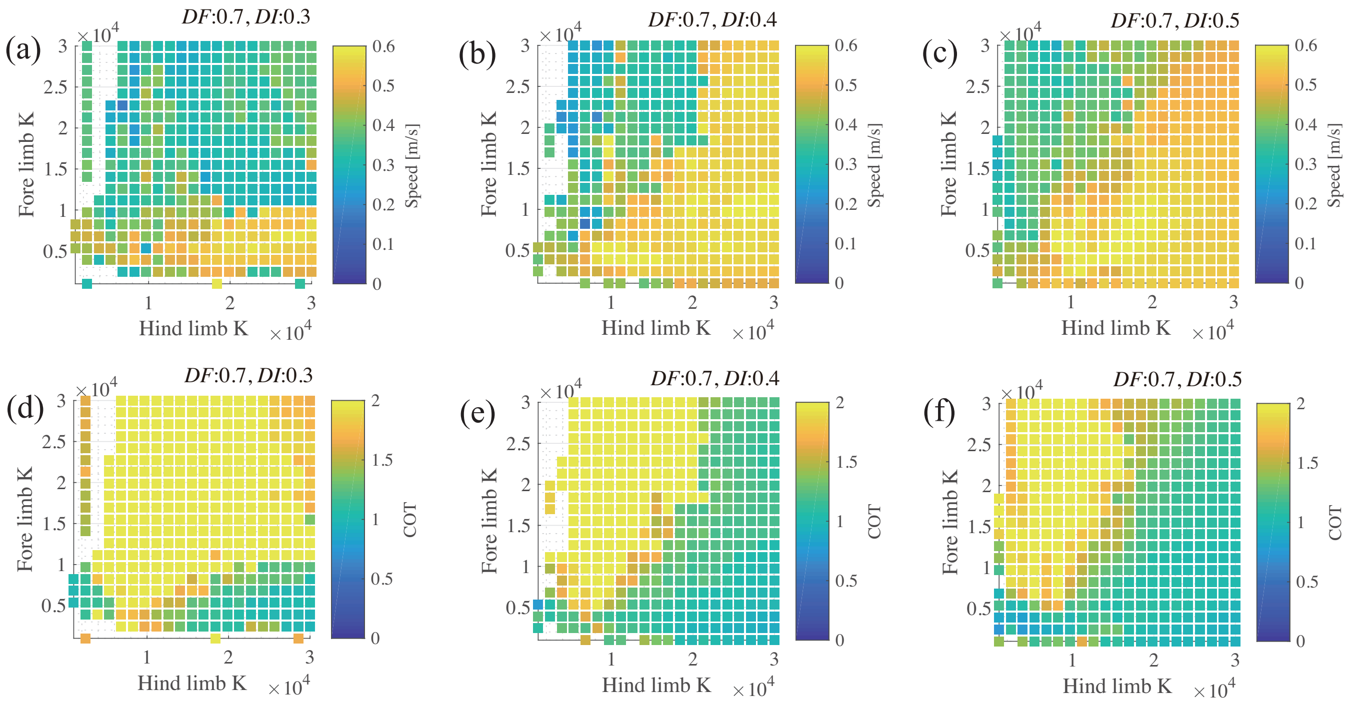

Fig. 6. Locomotor performance with various combinations of stiffness of proximal limb joints of shoulder and hip regions (K_v^{fore}, K_v^{hind}). Locomotion speeds for (a)$(DF, DI) = (0.7, 0.3)$, (b) $(DF, DI) = (0.7, 0.4)$, and (c) $(DF, DI) = (0.7, 0.5)$. Cost of transport for (d) $(DF, DI) = (0.7, 0.3)$, (e) $(DF, DI) = (0.7, 0.4)$, and (f) $(DF, DI) = (0.7, 0.5)$. Other parameters are set as shown in Table I. The white blank indicates that the robot fell while walking.

cost of transport (COT). To reduce the number of search parameters, we assume that $K_h^{fore(hind)} = 1/2 K_v^{fore(hind)}$ and that the other body parameters are the same as those listed in Table I.

A criterion, COT defined by [17], is calculated as follows:

$$\mathrm{COT} = \frac{1}{Dmg} \int_0^T P(t) \mathrm{d}t, \tag{10}$$

where D [m] is the distance traveled over a period T [s], m [kg] is the total mass of the robot, and g [m/s^2] is the gravitational acceleration. The power consumption of the actuator, P [W], is estimated by referring to [18], as follows:

$$P(t) = \sum_i \left(\chi(\tau_i(t)\dot{\theta}_i(t))) + \gamma \tau_i^2(t) \right), \tag{11}$$

$$\chi(z) = \begin{cases} 0 & (z \leq 0), \\ z & (z > 0), \end{cases} \tag{12}$$

where γ is a positive constant related to the energy consumption caused by heat emission. In this simulation, the constant values for the rotary and prismatic actuators, $\gamma^{\mathrm{rot}} = 0.001$ and $\gamma^{\mathrm{pri}} = 0.002$, respectively, are determined such that the positive work at the actuator becomes of almost the same order as that of the heat dissipation.

Figure 6 (a) and (d) shows the dependence of locomotion speed and COT on the proximal joints' stiffness during LS walking (i.e., $(DF, DI) = (0.7, 0.3)$). As shown in the above results (Fig. 4 and Fig. 5), the robot with a flexible shoulder and rigid hip (e.g., $(K_{\mathrm{v}}^{\mathrm{fore}}, K_{\mathrm{v}}^{\mathrm{hind}}) = (5.0 \times 10^3, 2.5 \times 10^4)$) achieves faster locomotion speed and efficient walking among other stiffness combinations. In contrast, the robot with a rigid shoulder and flexible hip exhibits unstable walking, and thus, falls down (e.g., $(K_{\mathrm{v}}^{\mathrm{fore}}, K_{\mathrm{v}}^{\mathrm{hind}}) = (2.5 \times 10^4, 5.0 \times 10^3)$). Note that the white blank observed in the results of the grid search (Fig. 6) indicates that the robot falls down due to unstable locomotion.

Furthermore, the different walking patterns produce a different tendency of the body properties on the locomotion performance. When the diagonality becomes $DI = 0.4$ and 0.5, as shown in Fig. 6 (b), (c), (e), and (f), the robot with a stiff shoulder and hip also achieves fast and efficient locomotion (e.g., $(K_{\mathrm{v}}^{\mathrm{fore}}, K_{\mathrm{v}}^{\mathrm{hind}}) = (2.5 \times 10^4, 2.5 \times 10^4)$). This is because the stride motions of the forelimbs and hindlimbs proceeded almost synchronously, making the discrepancy through the trunk smaller than that obtained by walking by $DI = 0.3$. The combination of rigid shoulder and flexible hip still exhibits low locomotor performance.

The above results suggest that the functionality of the shoulder hammock structure changes depending on the gait patterns for stable locomotion. During LS walking gait, where the forelimbs and hindlimbs generate vertical motion of the trunk independently, the flexibility of the shoulder hammock structure contributes to absorbing the discrepancy at the trunk. In contrast to the absorb function, during trotting(pacing) gait, where the diagonal(ipsilateral) forelimbs and hindlimbs move synchronously ($DI = 0.5$ or 0.0), the stiffness of the shoulder hammock structure should be high like the hip region, so that the dynamics of the forelimbs correspond to those of the hindlimbs for stable locomotion. This adjustment is the other functionality of the shoulder hammock structure, namely consistency of the white body. To change these functionalities, the stiffness of the shoulder hammock structure should be changed from soft to stiff during gait transition to walking to trotting(pacing).

IV. Conclusions and future work

The main contribution of this study is to demonstrate by using 2D simulation that the flexibility of translational motion of the shoulder in the sagittal plane moderates stable walking. Particularly, the simulation results suggest two fundamental functions of the shoulder hammock structure during various walking patterns. The first function is reconciliation of the inverted pendulum motions between the forelimbs and hindlimbs during LS walking. The second function is to correspond the stiffness of the forelimbs to that of the hindlimbs for stable trotting (pacing) gait (i.e., $DI = 0.5, 0.0$). These insights help us understand animals' shoulder hammock structure and its behaviors, because mammals show diversities in the shape and motion of the scapula depending on the species: feline families exhibit large range of motion of scapula, while horse families exhibit small range one [11], [19].

In addition to functionalities of the shoulder hammock structure during walking gait, the simulation results also suggest the possibility of stiffness control. The scapula is connected to the chest through many muscles. Therefore, the stiffness of the hammock structure is likely to change its physical property as the muscles around the knee can adjust the stiffness of the knee joint depending on the situation [20], [21]. We expect that our minimal model involving the hammock structure would shed new light on the control scheme for an agile legged robot that can exploit a flexible whole–body system.

For further work, we evaluate the functionalities of the shoulder hammock structure during the walking task by using the developed robot [12] as well as extend the model from 2D plane to 3D space. In 3D locomotion, we expect that the shoulder hammock structure may contribute the stability in the walking task. This is because the inverted–pendulum motion is a fundamental phenomenon in the legged locomotion in the both 2D plane and 3D space. Furthermore, we believe that the hammock structure would contribute to stability in rolling and twisting motions of the trunk: the trunk twists in trotting gait while it rolls in pacing gait. Besides, we will address the effects of the shoulder hammock structure during the high–speed running, landing task after leaping over some obstacles, and rapid turning [22], [23], [24].

ACKNOWLEDGMENT

This study was supported by the Japan Science and Technology Agency, CREST (JPMJCR14D5) and Tough Cyberphysical AI Research Center, TCPAI, Tohoku University. This study was also supported by JSPS KAKENHI Grant-in-Aid for Scientific Research on Innovative Areas "Science of Soft Robot" project under Grant Number JP18H05466.

Appendix A: Walking patterns for phase oscillators

To reflect the duty factor DF, this study employs different intrinsic angular velocities ω_{sw} and ω_{st} for the swing phase model and stance phase model for the phase oscillator. Each period of the swing and stance phases can be described as $T_{st} = \pi/\omega_{\text{sw}}$ and $T_{\text{st}} = \pi/\omega_{\text{st}}$, respectively. Therefore, the relation between ω_{sw} and ω_{st} is detected as follows:

$$\begin{aligned} T_{\text{st}} &= DF(T_{\text{sw}} + T_{\text{st}}), && \text{(A.1)}\\ \pi/\omega_{\text{st}} &= DF(\pi/\omega_{\text{sw}} + \pi/\omega_{\text{st}}), && \text{(A.2)}\\ DF\pi/\omega_{\text{sw}} &= (1-DF)\pi/\omega_{\text{st}}, && \text{(A.3)}\\ \omega_{\text{sw}} &= \frac{DF}{1-DF}\omega_{\text{st}}. && \text{(A.4)} \end{aligned}$$

Thus, the intrinsic angular velocity ω is described as follows:

$$\omega_i = \begin{cases} \omega_{\text{sw}} & (\sin\phi_i > 0), \\ \omega_{\text{st}} & (\sin\phi_i \le 0), \end{cases} \tag{A.5}$$

To reflect the diagonality DI, the initial phase ϕ_i^{init} for each oscillator is detected as follows:

$$\begin{aligned} \phi_0^{\text{init}} &= \phi_2^{\text{init}} - \Delta\phi_{\text{sw}}, && \text{(A.6)}\\ \phi_1^{\text{init}} &= \phi_3^{\text{init}} - \Delta\phi_{\text{st}}, && \text{(A.7)}\\ \phi_2^{\text{init}} &= \frac{\pi}{2}, && \text{(A.8)}\\ \phi_3^{\text{init}} &= \frac{3\pi}{2}, && \text{(A.9)} \end{aligned}$$

where $\Delta\phi_{\text{sw}}$ and $\Delta\phi_{\text{st}}$ are the specific phase differences between the fore and hindlimbs. Here, we assume that the bilateral limbs (e.g., left and right fore/hind limbs) move in anti-phase. The specific phase difference between the limbs is described as follows:

$$\Delta\phi_{\text{sw}} = \begin{cases} T_{\text{d}}\omega_{\text{sw}} & (T_{\text{d}}\omega_{\text{sw}} \le \pi/2), \\ \frac{\pi}{2} + (T_{\text{d}} - \frac{\pi/2}{\omega_{\text{sw}}})\omega_{\text{st}} & (T_{\text{d}}\omega_{\text{sw}} > \pi/2), \end{cases} \tag{A.10}$$

$$\Delta\phi_{\text{st}} = \begin{cases} T_{\text{d}}\omega_{\text{st}} & (T_{\text{d}}\omega_{\text{st}} \le \pi/2), \\ \frac{\pi}{2} + (T_{\text{d}} - \frac{\pi/2}{\omega_{\text{st}}})\omega_{\text{sw}} & (T_{\text{d}}\omega_{\text{st}} > \pi/2). \end{cases} \tag{A.11}$$

Here, the parameter T_{d} is the lag period between a hindlimb and forelimb on the ipsilateral side, which can be detected by DI, T_{sw}, and T_{st} values as follows:

$$T_{\text{d}} = DI(T_{\text{st}} + T_{\text{sw}}). \tag{A.12}$$

References

[1] SPOT, BostonDynamics, Available at: https://www.bostondynamics.com/spot, Accessed 22, Feb, 2020.
[2] Ghost Spirit Series, GostRobotics, Available at: https://www.ghostrobotics.io/robots, Accessed 22, Feb, 2020.
[3] Laikago, Unitree, Available at: http://www.unitree.cc, Accessed 22, Feb, 2020.
[4] S. B. Williams, A. M. Wilson, J. Daynes, K. Peckham, and R. C. Payne, Functional anatomy and muscle moment arms of the thoracic limb of an elite sprinting athlete: the racing greyhound (Canis familiaris), Journal of Anatomy, 213, pp. 373–382, 2008.
[5] S. B. Williams, A. M. Wilson, L. Rhodes, J. Andrews, and R. C. Payne, Functional anatomy and muscle moment arms of the pelvic limb of an elite sprinting athlete: the racing greyhound (Canis familiaris), Journal of Anatomy, 213, pp. 361–372, 2008.
[6] D. J. Dutto, D. F. Hoyt, H. M. Clayton, E. A. Cogger, and S. J. Witcker, Joint work and power for both the forelimb and hindlimb during trotting in the horse, Journal of Experimental Biology, 209, pp. 3990–3999, 2006.
[7] D. V. Lee, Effects of grade and mass distribution on the mechanics of trotting in dogs, Journal of Experimental Biology, 214, pp. 402–411, 2011.

[8] M. F. Bobbert and S. Santamaria, Contribution of the forelimbs and hindlimbs for the gorse to mechanical energy changes in jumping, Journal of Experimental Biology, 208, pp. 249–260, 2006.

[9] J. E. Bertram and A. Gutmann, Motion of the running horse and cheetah revisited: fundamental mechanics of the transverse and rotary gallop, Journal of The Royal Society Interface, 6, pp.549–559, 2015.

[10] M. Hildebrand and G. E. Jr. Goslow, Analysis of Vertebrate Structure, 5th edition. New York: Wiley, pp.635, 2001.

[11] P. D. Polly, Limbs in mammalian evolution, in *Fins into limbs: Evolution, development, and transformation*, B. K. Hall (edited), University of Chicago Press, pp. 245–268, 2007.

[12] A. Fukuhara, M. Gunji, Y. Masuda, K. Tadakuma, and A. Ishiguro, Development of quadruped robot that can exploit shoulder hammock structure, in Proceedings of IEEE/SICE SII2020, pp.1139–1143, 2020.

[13] E. Lahunta, Guide to the dissection of the dog (Eighth edition), SANDERS ELSEVIER, 2016.

[14] D. R. Carrier, S. M. Deban, and T. Fischbein, Locomotor function of the pectoral girdle 'muscular sling' in trotting dogs, The Journal of Experimental Biology, 209, pp. 2224–2237, 2006.

[15] M. Hildebrand, Symmetrical gait of horses, Science, 150(3697), pp. 701–708, 1965.

[16] M. Cartmill, K. Brown, C. Atkinson, E. A. Cartimill, E. Findley, D. G. Socoloske, A. H. Rose, and J. Mueller, The gait of marsupials and the evolution of diagonal–sequence walking in primates, American Journal of Physical Anthropology, 171, pp. 182–197, 2019.

[17] G. Gabrielli and T. V. Kármán: What price speed? specific power required for propulsion of vehicles. Mechanical Engineering, 72, pp.775–781, 1950.

[18] J. Nishii, K. Ogawa, and R. Suzuki: The optimal gait pattern in hexapods based on energetic efficiency. Proceedings of the 3rd International Symposium on Artificial Life and Robotics, pp. 106-109, 1998.

[19] G. Catavitello, Y. Lvanenko, and F. Lacquaniti, A kinematic synergy for terrestrial locomotion shared by mammals and birds, eLife, 2018;7:e38190, 2018.

[20] D. V. Lee, M. P. McGuigan, E H. Yoo, and A. A. Biewener, Compliance, actuation, and work characteristics of the goat foreleg and hindleg during level, uphill, and downhill running, Journal of Applied Physiology, 104, pp. 130–141, 2008.

[21] S. Kuitunen, P. V. Komi, and H. Kyr ol anen, Knee and ankle joint stiffness in sprint running,

[22] Z. Zhang, H. Yu, J. Yang, L. Wang, and L. Yang, How cat lands: insights into contribution of the forelimbs and hindlimbs to attenuating impact force, Chinese Science Bulletin, 59(26), pp. 3325–3332, 2014.

[23] M. Santello, Review of motor control mechanisms underlying impact absorption from falls, Gait and Posture, 21, pp. 85–94, 2005.

[24] A. N. Kuznetsov, O. S. Luchkina, A. A. Panyutina, and N. V. Kryukova, Observation on escape runs in wild European hare as a basis for the mechanical concept of extreme cornering with special inference of a role of the peculiar subclavian muscle, Mammalian Biology, 84, pp. 61–72, 2017.